Applied Energy 137 (2015) 913–924

Contents lists available at ScienceDirect

Applied Energy

journal homepage: www.elsevier.com/locate/apenergy

Longevity-conscious dimensioning and power management of the hybrid energy storage system in a fuel cell hybrid electric bus

Xiaosong Hu *, Lars Johannesson, Nikolce Murgovski, Bo Egardt

Department of Signals and Systems, Chalmers University of Technology, 41296 Gothenburg, Sweden

HIGHLIGHTS

- Hybrid energy storage system is optimally sized and controlled for a hybrid bus.
- Dynamic battery health model is incorporated in the optimization.
- Convex programming is efficient for optimizing hybrid propulsion systems.
- Optimal battery replacement strategy is explored.
- Comparison to the battery-only option is made in the health-aware optimization.

ARTICLE INFO

Article history:
Received 4 February 2014
Received in revised form 7 May 2014
Accepted 10 May 2014
Available online 28 May 2014

Keywords:
Hybrid energy storage system
Electrified vehicle
Component sizing
Energy management
Battery health
Convex optimization

ABSTRACT

Energy storage systems (ESSs) play an important role in the performance and economy of electrified vehicles. Hybrid energy storage system (HESS) combining both lithium-ion cells and supercapacitors is one of the most promising solutions. This paper discusses the optimal HESS dimensioning and energy management of a fuel cell hybrid electric bus. Three novel contributions are added to the relevant literature. First, efficient convex programming is used to simultaneously optimize the HESS dimension (including sizes of both the lithium-ion battery pack and the supercapacitor stack) and the power allocation between the HESS and the fuel cell system (FCS) of the hybrid bus. In the combined plant/controller optimization problem, a dynamic battery State-of-Health (SOH) model is integrated to quantitatively examine the impact of the battery replacement strategy on both the HESS size and the bus economy. Second, the HESS and the battery-only ESS options are systematically compared in the proposed optimization framework. Finally, the battery-health-perceptive HESS optimization outcome is contrasted to the ideal one neglecting the battery degradation (assuming that the battery is durable over the bus service period without deliberate power regulation).

1. Introduction

Automobiles are currently responsible for a considerable part of the word's primary energy consumption, mostly fossil fuels, leading to serious public concerns over energy sustainability and environmental benignity [1]. Improvement of the fuel economy of vehicle propulsion systems hence has become a top priority. As an important technology, electrified vehicles, such as battery electric vehicles (BEVs) and hybrid electric vehicles (HEVs), are being intensively investigated and developed by almost all the automotive companies over the world [2–4]. The performance, reliability, and cost effectiveness of these electrified vehicles are significantly influenced by the selection, integration, and control of energy storage systems (ESSs, onboard electricity carrier).

Lithium-ion battery and supercapacitor technologies are among the most appropriate ESS options for electrified vehicles [5,6]. Lithium-ion batteries often exhibit good energy/power characteristics, whereas their lifetime may need further improvement. Despite a very low energy density, supercapacitors typically have an extremely high power density and sufficient durability. By combining these two ESSs, a hybrid energy storage system (HESS) can be built up. It has been demonstrated in [7–9] that a synergistically enhanced overall performance could be expected for this type of dual buffer, owing to the prospect of mutually compensating deficiencies. HESS, nevertheless, results in an increased complexity that poises a heavy challenge for energy-buffer system integration and power management in electrified powertrains.

* Corresponding author. Address: E-building, Hörsalsvägen11, 41296 Gothenburg, Sweden. Tel.: +46 31 772 1538; fax: +46 31 772 1748.
E-mail address: xiaosong@chalmers.se (X. Hu).

http://dx.doi.org/10.1016/j.apenergy.2014.05.013
0306-2619/

The power coordination between an HESS and a prime mover (i.e., an internal combustion engine) of an HEV was simulated in ADVISOR, Advanced Vehicle Simulator [10]. Energy management of an HESS for a BEV was evaluated based on the simulation of urban driving schedules in MATLAB/SIMULINK environment [11]. A fuzzy-logic-based energy management strategy for an HESS of a BEV was also discussed in hardware-in-the-loop (HIL) experiments [12]. These studies illustrated that HESS can successfully meet the vehicular energy/power requirements, while reducing the battery stress with the load-leveling aid of supercapacitors. These strategies, however, were heuristic rule-based control algorithms that cannot realize the optimum power allocation between multiple energy sources with respect to some criterions, e.g., energy-consumption minimization. The consequent non-optimal power management may not make the most of the HESS potential and benefits, which in the worst case incurs incorrect decisions in the product planning.

The advantages of optimization-based energy controls over conventional rule-based ones have been indicated in [13–16]. Optimal energy management strategies are often used for benchmarking those online implementable algorithms, e.g., rule-based methods. In other words, the optimized control law informs designers of the potential of improving vehicle performance and guides them to refine existing causal/implementable strategies. Powertrain optimization has become a vast area of intensive research, as a result of great motivations for pursuing maximum system benefits. An optimal power management strategy, for example, was obtained by dynamic programming (DP), in order to minimize the fuel consumption of a parallel HEV equipped with an HESS [17]. The foregoing articles, however, did not involve the HESS dimensioning problem, an additional instrumental factor influencing the drivability and economy of electrified powertrains. First insights have been provided in [18–20] that the optimal supervisory energy control law is strongly coupled with the powertrain component sizing, and a framework of simultaneously optimal sizing and energy management is thereby needed for achieving an "exactly" optimal solution. An integrated optimization approach was applied to derive the optimal HESS size and control strategy for a BEV [21]. In this approach, a bi-loop optimization topology was used, where the optimal HESS size was searched in the outer loop, while a three-mode rule-based power distribution strategy is optimized in the inner loop. Although the parameters of the rule-based control algorithm are tuned in the inner loop, the control policy/feedback was not inherently optimal, since the controller structure was decided by the rules. Moreover, the bi-loop optimization may be very computationally expensive. A nonlinear programming problem was also formulated to simultaneously solve the optimal HESS size and energy management for minimizing the total cost of ownership of a BEV [22]. Although the solver on the basis of the interior-point algorithm could quickly solve this problem, the solution was highly prone to getting stuck in local minima, since the combined plant/controller optimization problem was quite complicated and nonlinear. Therefore, the nonlinear-programming-based method lacked a guarantee of global optimality. In our prior work [23], the innovative convex programming was employed to accomplish the simultaneously optimal HESS size and power management strategy for a series hybrid powertrain. It has been verified that the convex optimization can rapidly and efficiently yield a globally optimal solution.

All of the aforementioned papers regarding the HESS optimization overlook the potential implications of the battery health. In other words, the existing formulations of the HESS optimization were unconscious of the State-of-Health (SOH) of the battery that is actually closely tied to the HESS sizing and the supervisory control strategy design of electrified powertrains. As a consequence, a quantitative examination of the battery replacement strategy over vehicle service period was lacked. Some interesting questions also remained unaddressed. For instance, how large should the optimized HESS be if no battery replacement is required? What if the battery is replaced twice? And what is the preferred replacement strategy?

This paper is concerned with the optimal HESS dimensioning and energy management of a fuel cell hybrid electric bus. Its main purpose is to attempt to explore solutions to the above interesting questions. The convex optimization for HEVs/PHEVs energy management and sizing was firstly proposed in our previous work [16,20,23–25] for various vehicle configurations and driving cycles. The emphasis of this article is to utilize convex programming for optimization of a fuel cell/HESS bus, and to the best of our knowledge, this is the first time that convex programming extends to fuel cell/HESS vehicles. To sufficiently demonstrate the efficacy of the approach and to showcase the value of the obtained results, three prominent important contributions are delivered to the relevant literature: (1) battery-health-aware optimization of the HESS dimension and the power distribution between the HESS and the fuel cell system (FCS) via convex programming; (2) a comparison of the HESS and the battery-only ESS options in the context of battery degradation; and (3) a comparison between the battery-health-conscious HESS optimization result and the ideal counterpart neglecting the battery capacity fading.

The remainder of the paper is outlined as follows: Section 2 elaborates the modeling of the propulsion system of the fuel cell hybrid bus; the battery SOH model is described in Section 3; the convex-programming-based framework is formulated in Section 4 for the combined HESS size and power management optimization taking the battery SOH into account; Section 5 illustrates the optimization results with different battery replacement strategies; a comparison with the battery-health-unaware scenario (the ideal case neglecting the battery wear) is carried out in Section 6 followed by further discussion in Section 7 and conclusions presented in Section 8.

2. Modeling of fuel cell hybrid bus powertrain

The architecture of the propulsion system of a fuel cell hybrid electric bus operated in Gothenburg, Sweden, is shown in Fig. 1. The bus is impelled by an electric machine (EM) with a power rating of 220 kW. A 100 kW unpressurized proton-exchange-membrane (PEM) FCS and an HESS constitute the main power sources of the bus. A DC–DC converter is applied to regulate the FCS

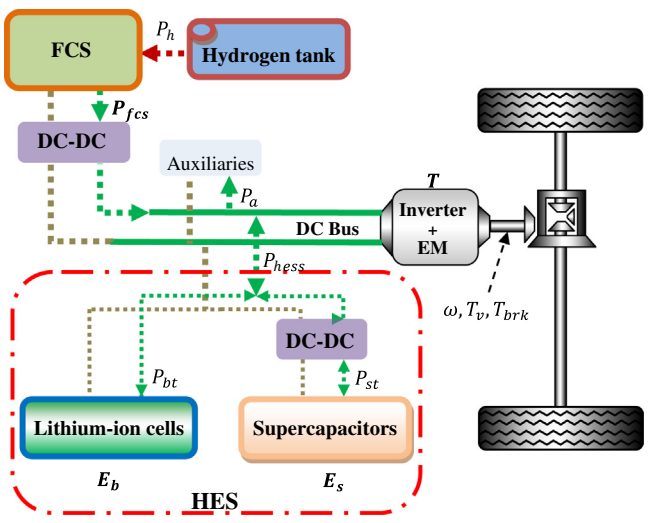

Fig. 1. Architecture of the fuel cell hybrid bus propulsion system.

current flow into the DC bus, to which the HESS is connected in parallel. The difference between the current demand from the EM inverter and the current flow from the FCS DC–DC converter is offset by the HESS composed of a lithium-ion battery pack and a supercapacitor pack. Owing to the nature of large voltage fluctuation, another DC–DC converter is used to control the voltage of the supercapacitor pack to match the paralleled battery pack. The bus is driven on a bus line in Gothenburg, Sweden, which is characterized by velocity and slope profiles shown in Fig. 2. In order to guarantee a rapid simulation with adequate precision, the quasi-static modeling methodology is used to model the hybrid powertrain [14,16]. The power request at the wheels can be readily interpreted as an angular velocity $\omega(t)$ and a torque $T_v(t)$ on the shaft between the EM and the final drive, based on the longitudinal vehicle dynamics (please refer to [24] for more details). The EM torque $\boldsymbol{T}(t)$ is able to both meet the torque requirement for propelling and permit regenerative braking. However, when either its torque threshold $T_{min}(\omega(t))$ or the battery charge or current limit is violated, the friction braking $T_{brk}(t)$ will serve as a complement. The torque and power balance equations are represented as

$$\begin{aligned} &\boldsymbol{T}(t) = T_v(t) - T_{brk}(t) \\ &P_m(t) + P_{loss,m}(t) + P_a(t) = P_{hess}(t) + \boldsymbol{P_{fcs}}(t)\eta_{dc} \end{aligned} \tag{1}$$

where P_m is the EM power acting on the final drive calculated by

$$P_m(t) = \boldsymbol{T}(t)\omega(t). \tag{2}$$

The EM loss $P_{loss,m}$ (including the inverter loss) is described by a quadratic function of torque

$$P_{loss,m}(t) = b_0(\omega)\boldsymbol{T}^2(t) + b_1(\omega)\boldsymbol{T}(t) + b_2(\omega) \tag{3}$$

where $b_l (l = 0, 2)$ are nonnegative speed-dependent coefficients. The quadratic loss function that gives a good fit is adopted to preserve the subsequent optimization problem convexity, and the optimization variables are highlighted in bold (see Section 4). The efficacy of convexifying the EM has been proven in [16,20,23–25]. The EM efficiency and the torque thresholds are given in Fig. 3. In Eq. (1), P_a and $\boldsymbol{P_{fcs}}$ are the power for the bus auxiliary devices (excluding the auxiliary system of the FCS) and the FCS net power, respectively. The terminal HESS power P_{hess} is computed by

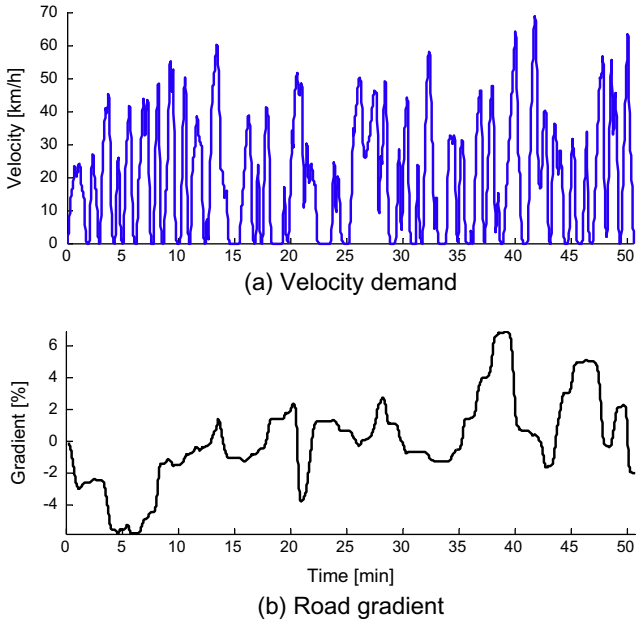

Fig. 2. Bus line: (a) velocity demand; and (b) road slope.

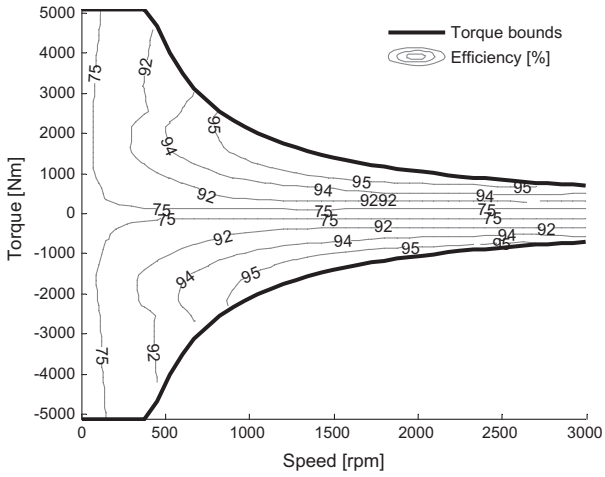

Fig. 3. EM efficiency and torque thresholds: the thin lines are efficiency, and the thick lines represent the torque limits.

$$P_{hess}(t) = \begin{cases} P_{bt}(t) + P_{st}(t)\eta_{dc}, & P_{st}(t) \geqslant 0 \\ P_{bt}(t) + \frac{P_{st}(t)}{\eta_{dc}}, & P_{st}(t) < 0 \end{cases} = P_{bt}(t) + \min\left(P_{st}(t)\eta_{dc}, \frac{P_{st}(t)}{\eta_{dc}}\right) \tag{4}$$

where P_{bt} and P_{st} represent the terminal powers of the battery pack and the supercapacitor stack, respectively. The discharge power is assumed to be positive, by convention. The parameter η_{dc} denotes the efficiency for both DC–DC converters. As in [16,20], for simplicity, η_{dc} and P_a are assumed to be constant (i.e., a cycle-averaged converter efficiency is considered).

The hydrogen-consumption map as a function of the FCS net power is approximated by a quadratic function as follows:

$$P_h(t) = a_0\boldsymbol{P}_{\boldsymbol{fcs}}^2(t) + a_1\boldsymbol{P_{fcs}}(t) + a_2 \tag{5}$$

with $a_j \geqslant 0, j \in \{0, 2\}$, and P_h being the hydrogen power of the FCS. The quasi-static model of the FCS and its corresponding approximated model are shown in Fig. 4. The original FCS model is acquired in Advanced Vehicle Simulator (ADVISOR, a scaled version of FC_ANL50H2). It is clear that the fitted quadratic function can simulate the FCS hydrogen consumption with very high accuracy. Quadratic FCS models have also been used in [26,27] for system-level powertrain analysis.

The lithium-ion battery and supercapacitor packs comprise strings in parallel, with each string containing the same number of cells connected in series, as shown in Fig. 5. Each cell is modeled by an open circuit voltage (OCV), $u_i, i \in \{b, s\}$, in series with a resistor, R_i, where the subscripts b and s refer to the battery and the supercapacitor, respectively.

The terminal pack power is calculated by

$$P_{it}(t) = \left(u_i(t)I_i(t) - R_iI_i^2(t)\right)\boldsymbol{n_i}, \quad i \in \{b, s\} \tag{6}$$

where I_i is the cell current, and $\boldsymbol{n_i}$ is the total number of cells. In this paper, an approximated affine OCV–SOC (State-of-Charge) model

$$u_i(t) = \frac{Q_i}{C_i}soc_i(t) + u_{i0}, \quad i \in \{b, s\} \tag{7}$$

is employed, which gives a good fit within the typically allowed battery SOC range for HEVs (see Fig. 6, A123's ANR26650m1 lithium–iron-phosphate battery cell is herein considered). In Eq. (7), Q_i represents the rated cell capacity in (As), and C_i and u_{i0} are coefficients in (F) and (V), respectively. Notice that Eq. (7) exactly defines the supercapacitor cell OCV, with $u_{s0} = 0$. The affine OCV model results in a convex HESS model, in which the internal pack power (without considering loss) $\boldsymbol{P_i}(t) = \boldsymbol{n_i}u_i(t)I_i(t)$ is used as an optimization variable. The associated pack energy E_i thereby can be expressed as

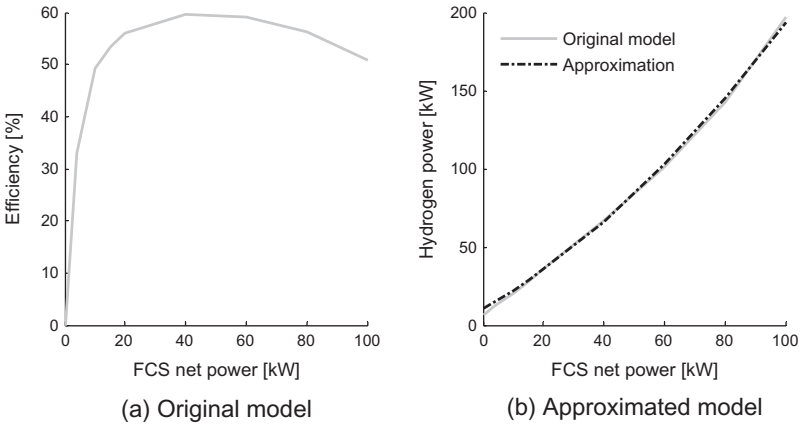

Fig. 4. Quasi-static FCS modeling: (a) efficiency of original model; and (b) approximate model.

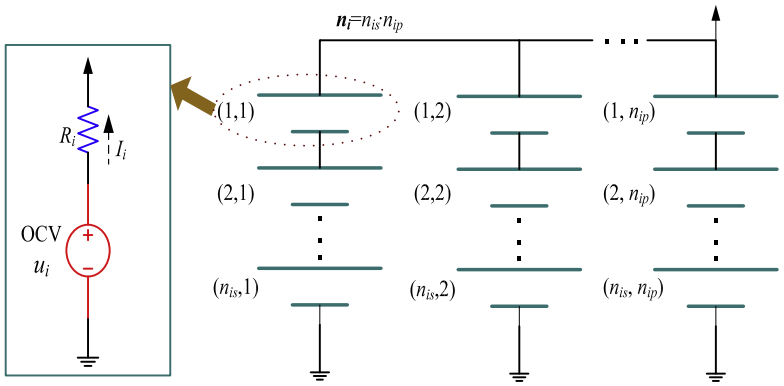

Fig. 5. Battery/supercapacitor pack configuration.

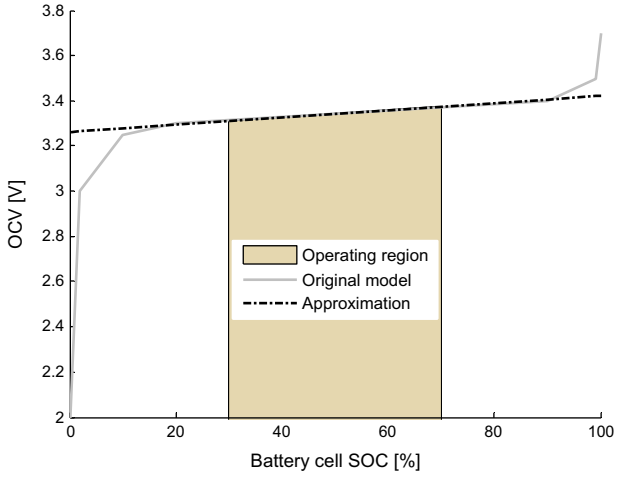

Fig. 6. Original and affine battery cell OCV–SOC models (A123's ANR26650m1 cell).

$$\begin{aligned}\boldsymbol{E_i}(t) &= \boldsymbol{n_i}Q_i\int_0^{soc_i(t)} u_i(t)dsoc_i(t)\\ &= \boldsymbol{n_i}Q\int_0^{soc_i(t)}\left(\frac{Q_i}{C_i}soc_i(t)+u_{i0}\right)dsoc_i(t)\\ &= \boldsymbol{n_i}Q_i\left(\frac{Q_i}{2C_i}soc_i^2(t)+u_{i0}soc_i(t)\right)\\ &= \frac{\boldsymbol{n_i}C_i}{2}\left(u_i^2(t)-u_{i0}^2\right), i\in\{b,s\}.\end{aligned} \tag{8}$$

Then, substituting the OCV as a function of energy from Eq. (8) into Eq. (6) yields the terminal pack power

$$P_{it}(t) = \boldsymbol{P_i}(t) - \frac{R_iC_i\boldsymbol{P_i^2}(t)}{2\boldsymbol{E_i}(t)+u_{i0}^2C_i\boldsymbol{n_i}}, \quad i\in\{b,s\} \tag{9}$$

which is a concave function of $\boldsymbol{P_i}(t)$, $\boldsymbol{E_i}(t)$, and $\boldsymbol{n_i}$, provided that $\boldsymbol{E_i}(t)$ and $\boldsymbol{n_i}$ are nonnegative real values. The terminal HESS power, Eq. (4), thus can be rewritten as a concave function of $\boldsymbol{P_i}(t)$, $\boldsymbol{E_i}(t)$, and $\boldsymbol{n_i}$. Several pack constraints are necessary, including the bounds on the cell current (I_{imin} and I_{imax}), the SOC restrictions (soc_{imin} and soc_{imax}), and the charge sustenance for HEVs. Incorporating the cell dynamics, all the constraints are reformulated as convex with respect to $\boldsymbol{P_i}(t)$, $\boldsymbol{E_i}(t)$, and $\boldsymbol{n_i}$ as follows:

$$\begin{cases}\frac{d\boldsymbol{E_i}(t)}{dt} = -\boldsymbol{P_i}(t)\\ I_{imin}\sqrt{\boldsymbol{n_i}\left(\frac{2\boldsymbol{E_i}(t)}{C_i}+u_i0^2\boldsymbol{n_i}\right)} \leqslant \boldsymbol{P_i}(t) \leqslant I_{imax}\sqrt{\boldsymbol{n_i}\left(\frac{2\boldsymbol{E_i}(t)}{C_i}+u_{i0}^2\boldsymbol{n_i}\right)}\\ \frac{C_i\boldsymbol{n_i}}{2}\left(u_i^2(soc_{imin})-u_{i0}^2\right) \leqslant \boldsymbol{E_i}(t) \leqslant \frac{C_i\boldsymbol{n_i}}{2}\left(u_i^2(soc_{imax})-u_{i0}^2\right)\\ \boldsymbol{E_i}(t_0) = \boldsymbol{E_i}(t_f) = \boldsymbol{E_i}(soc_i(t_0)), \quad \forall t\in[t_0,t_f], \quad i\in\{b,s\}\end{cases} \tag{10}$$

where t_0 and t_f are the initial and final times of driving cycle, respectively.

The mass of the HESS is scaled by

$$m_{hess} = \boldsymbol{n_b}m_b + \boldsymbol{n_s}m_s + m_p \tag{11}$$

where m_b and m_s are the battery cell mass and the supercapacitor mass, respectively. m_p is the additional mass associated with packaging and circuitry (including the supercapacitor DC–DC converter), which is assumed to account for 12.3% of the total mass of the HESS

(the detailed justification is referred to [28]). When sizing the HESS, this study concentrates on the optimal power ratings and energy capacity of the individual packs as non-quantized values, which is accomplished by relaxing $\boldsymbol{n_i}$ to a positive real value, as treated in [20,23–25]. Put another way, the battery and supercapacitor technologies are presumed to allow fabricating and assembling cells in accordance with the optimized pack power and energy content.

3. Battery SOH model

Battery degradation always occurs during realistic vehicle operation, and its fading rate depends on a multitude of factors. In [29], aging tests considering different current rates (*C*-rates), temperatures, and depths-of-discharge were made for A123's lithium–iron-phosphate battery cells (ANR26650m1). It has been found that the capacity fade of this type of cells highly depends on the current rate and the temperature, whereas the depth-of-discharge factor is negligible. Furthermore, a correlation between the capacity loss and the discharged ampere-hour throughput has been calibrated by the following semi-empirical model:

$$\Delta Q_b = M(c)\exp\left(\frac{-E_a(c)}{RT_e}\right)A(c)^z \tag{12}$$

where ΔQ_b is the percentage of capacity loss in (%), c is the *C*-rate, and M is the pre-exponential factor as a function of the *C*-rate, as shown in Table 1. The ideal gas constant is denoted by R (i.e., 8.31 J/mol·K), T_e is the lumped battery temperature in (K), and A is the discharged ampere-hour (Ah) throughput depending on the *C*-rate. The activation energy E_a in (J/mol) and the power-law factor z are identified by

$$\begin{cases} E_a(c) = 31700 - 370.3c, \\ z = 0.55. \end{cases} \tag{13}$$

Note that in order to assign the same discharge current to all the battery cells for reducing the complexity of experimentation, the *C*-rate c is defined in [29] with respect to a de-rated capacity of 2 Ah.

The capacity loss of 20% ($\Delta Q_b = 20$) is often indicative of the end-of-life (EOL) of an automotive battery, and the corresponding total discharged Ah throughput A_{tol} is, therefore, algebraically calculated by

$$A_{tol}(c) = \left[\frac{20}{M(c)\exp\left(\frac{-E_a(c)}{RT_e}\right)}\right]^{1/z}. \tag{14}$$

Then, the total Ah throughput including both the charge and discharge processes equals to $2A_{tol}$, and the number of cycles until the battery EOL, N, is attained by

$$N(c) = \frac{2A_{tol}(c)}{\frac{2Q_b}{3600}} = \frac{3600A_{tol}(c)}{Q_b} \tag{15}$$

where one cycle corresponds to an ampere-second throughput of $2Q_b$. As in [30,31], based on Eqs. (14) and (15), an energy throughput based battery state of health model can be established below:

$$\begin{aligned} soh(t) &= 1 - \frac{1}{2N(c)Q_b\bar{u}_b}\int_0^t |I_b(\tau)\bar{u}_b|d\tau \\ &= 1 - \frac{1}{2N(c)E_{nb}}\int_0^t |P_{nb}(\tau)|d\tau \end{aligned} \tag{16}$$

Table 1
Pre-exponential factor as a function of the *C*-rate.

[a]*C*-rate c	0.5	2	6	10
M	31,630	21,681	12,934	15,512

[a] 1 *C*-rate corresponds to 2 A [29].

where $\bar{u}_b$ is the nominal voltage of the battery cell (i.e., 3.3 V), $P_{nb} = I_b\bar{u}_b$ is the nominal internal power, and $E_{nb} = Q_b\bar{u}_b$ is the energy capacity in (Ws). Once $soh(t) = 0$, the battery EOL (i.e., 20% capacity loss) is reached. Given $c = \frac{|P_{nb}|Q_b}{2E_{nb}}$, the derivative of Eq. (16) can be written as

$$\frac{dsoh(t)}{dt} = \frac{-|P_{nb}(t)|}{2N(|P_{nb}(t)|)E_{nb}}. \tag{17}$$

As argued in [18,30], it is reasonable to assume that the lumped battery temperature T_e is kept constant by an advanced thermal management system. In this paper, $T_e = 298.15K$ (room temperature, 25 °C) is considered, which is often recommended by the battery manufacturers (the battery specification typically corresponds to this temperature [18]). The associated SOH model, Eq. (17), is accurately approximated by the following three piecewise quadratic functions

$$\frac{dsoh(t)}{dt} = \begin{cases} d_{0,1}P_{nb}^2(t) + d_{1,1}, & |P_{nb}(t)| \leqslant 40.31 \\ d_{0,2}P_{nb}^2(t) + d_{1,2}, & 40.31 < |P_{nb}(t)| \leqslant 57.14 \\ d_{0,3}P_{nb}^2(t) + d_{1,3}, & |P_{nb}(t)| > 57.14 \end{cases} \tag{18}$$

where $d_{0,k}, k \in \{1,2,3\}$, are all negative. The original and approximate SOH models are shown in Fig. 7. It is apparent that the larger the battery power, the greater the absolute fading rate of the SOH with respect to time. It is worth pointing out that more cycles can be applied to the battery at an intermediate power level in comparison to the case at low power, because of calendar-life effects [30,31]. In other words, one cycle at low power consumes relatively long time.

Since the battery cell has a very flat OCV curve in the allowed SOC window (see Fig. 6), $\boldsymbol{P_b}(t) \approx \boldsymbol{n_b}P_{nb}(t)$. Using a variable change $\overline{\boldsymbol{soh}}(t) = \boldsymbol{n_b}soh(t)$, Eq. (18) can be rewritten as

$$\frac{d\overline{\boldsymbol{soh}}(t)}{dt} - d_{0,k}\frac{\boldsymbol{P_b^2}(t)}{\boldsymbol{n_b}} - \boldsymbol{n_b}d_{1,k} = 0, \quad k \in \{1,2,3\} \tag{19}$$

which is convex because $\boldsymbol{n_b} > 0$ and $\frac{\boldsymbol{P_b^2}(t)}{\boldsymbol{n_b}}$ is a quadratic-over-linear elementary convex function. Additionally, according to the number of battery replacements n_r, the SOH decrease over one driving cycle is constrained by

$$\overline{\boldsymbol{soh}}(t_0) - \overline{\boldsymbol{soh}}(t_f) = \boldsymbol{n_b}\Delta soh, \tag{20}$$

with

$$\Delta soh = \frac{L_d(n_r+1)}{L_a y_{bus}} \tag{21}$$

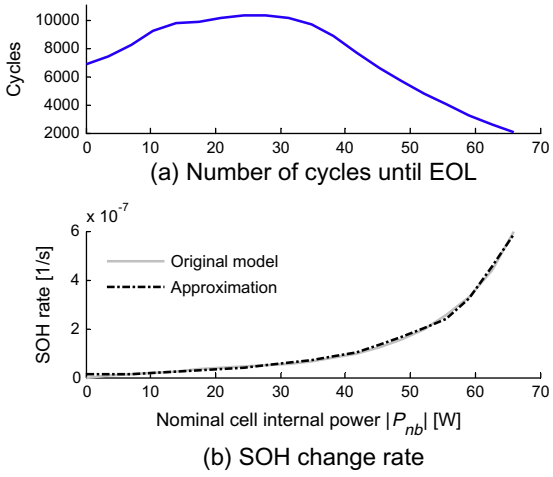

Fig. 7. Original and approximate SOH models: (a) number of cycles until EOL, N; and (b) SOH change rate, the negative derivative of the SOH.

where L_d is the length of driving cycle, L_a is the average distance traveled annually, and y_{bus} is the bus service period.

4. Convex optimization framework for HESS sizing and energy management

The convex objective function G, which is greatly concerned by the bus operators, is formulated to minimize a summation of the hydrogen and HESS costs:

$$G = \frac{c_h}{C_h}\int_{t_0}^{t_f} P_h(t)dt + c_{be}\boldsymbol{n_b} + c_{se}\boldsymbol{n_s} \tag{22}$$

where c_h is the hydrogen cost per gram in (Euro), C_h is the lower heating value of hydrogen in (J/g). The equivalent expenses of the battery c_{be} and the supercapacitor c_{se} are the cycle-normalized costs (i.e., the purchasing cost times the percentage of the driving-cycle length with respect to the distance traveled until the buffer EOL). Both the battery and the supercapacitor are paid with 5% yearly interest rate over their lifetimes, resulting in

$$\begin{cases} c_{be} = c_b E_{nb}\left(1+5\%\cdot\frac{1+\frac{y_{bus}}{n_r+1}}{2}\right)\frac{L_d}{L_a\frac{y_{bus}}{n_r+1}} = c_b E_{nb}\left(1+5\%\cdot\frac{n_r+y_{bus}+1}{2n_r+2}\right)\frac{L_d(n_r+1)}{L_a y_{bus}} \\ c_{se} = c_s C_s\left(1+5\%\cdot\frac{1+y_{bus}}{2}\right)\frac{L_d}{L_a y_{bus}} \end{cases} \tag{23}$$

where c_b and c_s are the battery price per Ws and the supercapacitor price per farad, respectively (packaging, circuitry, and supercapacitor DC–DC converter are included). A lifespan equivalent of the bus service period is herein considered for the supercapacitor pack, since there are virtually no concerns on its durability in vehicular applications.

The optimization variables are $\boldsymbol{P_{fcs}}(t)$, $\boldsymbol{T}(t)$, $\boldsymbol{P_b}(t)$, $\boldsymbol{E_b}(t)$, $\boldsymbol{n_b}$, $\overline{\boldsymbol{soh}}(t)$, $\boldsymbol{P_s}(t)$, $\boldsymbol{E_s}(t)$, and $\boldsymbol{n_s}$. The constraints are the vehicle power balance Eq. (1), the battery and supercapacitor constraints Eq. (10), the battery SOH constraints Eqs. (19) and (20), the EM torque limits, the FCS power limits, $\boldsymbol{n_b} \geqslant 0$, and $\boldsymbol{n_s} \geqslant 0$. Relaxing Eq. (1) to inequalities gives a convex problem (in which only affine equalities are allowed), without qualitatively altering the original problem as follows:

$$\begin{aligned} &\boldsymbol{T}(t) \geqslant T_v(t) \\ &P_m(t) + P_{loss,m}(t) + P_a(t) \leqslant P_{hess}(t) + \boldsymbol{P_{fcs}}(t)\eta_{dc} \end{aligned} \tag{24}$$

where $P_{hess}(t)$ is calculated by Eq. (4) with $P_{bt}(t)$ and $P_{st}(t)$ from Eq. (9). Moreover, relax Eq. (19) to inequalities

$$\frac{d\overline{\boldsymbol{soh}}(t)}{dt} - d_{0,k}\frac{\boldsymbol{P_b^2}(t)}{\boldsymbol{n_b}} - \boldsymbol{n_b}d_{1,k} \leqslant 0, \quad k \in \{1,2,3\}. \tag{25}$$

The justification behind Eq. (25) is that one of the three constraints must be active at every time instant for the optimal solution, because the battery wear influences the optimal design. Otherwise, an unnecessarily excessive decline in battery health would appear, inducing a more costly (non-optimal) solution.

The convex optimization framework is summarized in Table 2. The values of the so-called expressions in the table are accessed by the pertinent equations mentioned above. A tool, CVX [32], [33], is applied to parse the optimization problem to a general semi-definite program (SDP) that is amenable to the efficient solver, SeDuMi [34]. The convexity of the problem guarantees a globally optimal solution. More theoretical and algorithmic properties of convex programming are elucidated in [32].

The key parameters of the hybrid bus are given Table 3, while the main specifications of the onboard power sources are listed in Table 4. The supercapacitor technology (Maxwell BCAP 2000) for hybrid and electric vehicles is employed in this study.

5. Optimization results with different replacement strategies

5.1. Optimal battery replacement strategy

The convex optimization framework as shown in Table 2 can be efficiently implemented to achieve the HESS sizing results for different battery replacement strategies. The cycle-normalized costs of the hybrid bus considering up to four replacements are given in Fig. 8. It can be seen that as the replacement number increases, the total cost becomes larger, despite a slightly decreasing HESS cost, owing to obviously increasing hydrogen consumption. The corresponding HESS sizes are shown in Fig. 9. It is clear that the optimized battery size reduces with respect to the increasing replacement number, as opposed to that of the supercapacitor pack. Notice that for simplicity and better readability, the scenarios with more than four replacements are not discussed here, because they follow the change patterns observed in Figs. 8 and 9. The most cost-effective (optimal) strategy is, therefore, to use a relatively

Table 2
Convex optimization framework for combined HESS dimensioning and control.

(1)	The driving cycle, vehicle parameters, and the number of battery replacements n_r are firstly specified
(2)	For $q = 1,\ldots, N_d$, with N_d corresponding to the final time step of the driving cycle, do the optimization below
	Optimization variables: $\boldsymbol{P_{fcs}}, \boldsymbol{T}, \boldsymbol{P_b}, \boldsymbol{E_b}, \boldsymbol{n_b}, \overline{\boldsymbol{soh}}, \boldsymbol{P_s}, \boldsymbol{E_s}, \boldsymbol{n_s}$ ($\boldsymbol{P_{fcs}}, \boldsymbol{T}, \boldsymbol{P_b}$, and $\boldsymbol{P_s}$ are vectors of length N_d; $\boldsymbol{E_b}, \overline{\boldsymbol{soh}}$, and $\boldsymbol{E_s}$ are vectors of length N_d+1)
	Expressions: $P_h, P_m, P_{loss,m}, P_{hess}$, and $G = \sum_{q=1}^{N_d}\frac{c_h}{C_h}P_h(q)\Delta t + c_{be}\boldsymbol{n_b} + c_{se}\boldsymbol{n_s}$
	Objective function: G
	Constraints: Eqs. (10), (20), (24), and (25), as well as the following affine bounds
	$T_{min}(w(q)) \leqslant \boldsymbol{T} \leqslant T_{max}(w(q)), \quad 0 \leqslant \boldsymbol{P_{fcs}} \leqslant P_{max,fcs}, \quad \boldsymbol{n_b} \geqslant 0$, and $\boldsymbol{n_s} \geqslant 0$

Table 3
Key parameters of the hybrid bus.

Parameter	Value	Parameter	Value
Frontal area (m^2)	7.54	EM inertia (kgm^2)	2.3
Aerodynamic drag coefficient	0.7	Inertia of final drive and wheels (kgm^2)	41.8
Air density (kg/m^3)	1.184	Vehicular auxiliary power P_a (kW)	7
Rolling resistance coefficient	0.007	Length of driving cycle L_d (km)	16.55
Wheel radius (m)	0.509	Average annual mileage L_a (km)	50,000
Final gear	4.7	Bus service period y_{bus} (year)	5
Vehicle mass excluding HESS (ton)	14.5		

Table 4
Main specifications of the onboard power sources.

Parameter	Value	Parameter	Value
[a]Hydrogen price c_h (€/g)	0.00444	[d]Battery cell resistance R_b (ohm)	0.01
[b]Hydrogen lower heating value C_h (J/g)	120,000	[d]Battery cell mass m_b (kg)	0.07
Rated FCS power $P_{max,fcs}$ (kW)	100	[f]Supercapacitor price c_s (€/F)	0.01
[c]Battery price c_b (€/Ws)	0.00025	[g]Supercapacitor capacitance C_s (F)	2000
[d]Nominal battery capacity Q_b (As)	8280	[g]Maximum supercapacitor discharge I_{smax} (A)	1600
[d]Nominal battery voltage $\ddot{u}_b$ (V)	3.3	[g]Maximum supercapacitor charge I_{cmin} (A)	−1600
[e]Maximum battery discharge I_{bmax} (A)	70	Initial supercapacitor SOC $soc_s(t_0)$ (%)	50
[e]Maximum battery charge I_{bmin} (A)	-35	Maximum supercapacitor SOC soc_{smax} (%)	90
Initial battery SOC $soc_b(t_0)$ (%)	50	Minimum supercapacitor SOC soc_{smin} (%)	20
Maximum battrey SOC soc_{bmax} (%)	70	[g]Supercapacitor cell resistance R_s (ohm)	0.00035
Minimum battery SOC soc_{bmin} (%)	30	[g]Supercapacitor cell mass m_s (kg)	0.36
Initial battery SOH $soh(t_0)$	1	Average DC–DC efficiency η_{dc} (%)	96

[a] Adapted from [35] for Swedish case.
[b] Adopted from ADVISOR.
[c] Adopted from [23].
[d] Adopted from [36].
[e] Adopted from [30].
[f] Adopted from [23].
[g] Adopted from [37].

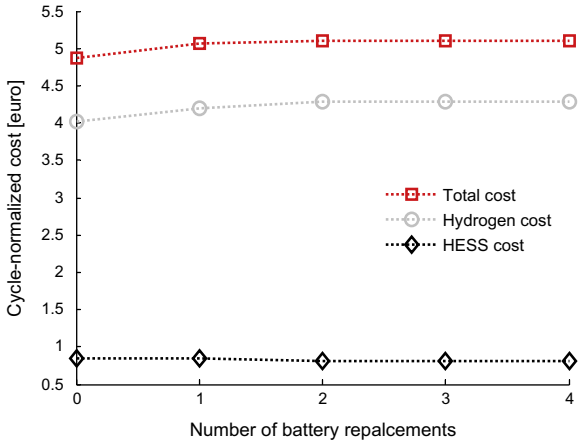

Fig. 8. Cycle-normalized costs of the optimized hybrid bus with different battery replacement strategies.

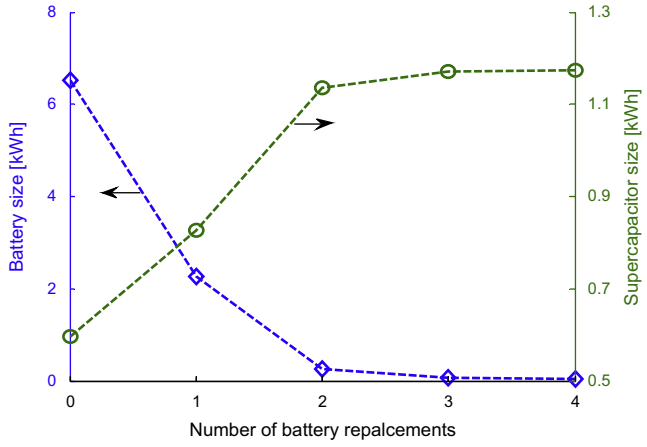

Fig. 9. Optimized HESS sizes with different battery replacement strategies.

large battery in the HESS ensuring no battery replacement over the bus service period.

The optimal replacement strategy is further contrasted to the one-replacement case (an example of the non-optimal strategies), in terms of the vehicular power split (see Fig. 10). It can be found that the larger battery pack in the optimal strategy results in more energy recuperated during the bus deceleration (particularly on the long downgrade before 500 s), which contributes to a higher hydrogen economy, as indicated in Fig. 8. The larger supercapacitor pack in the one-replacement strategy is not very helpful to improving the recovery of braking energy, because of its extremely low specific energy (see the instantaneous charge spikes in subplot (c) of Fig. 10).

The battery cell SOH trajectories under different replacement strategies are illustrated in Fig. 11. It is apparent that the increase of the replacement number leads to an enlarged SOH fade, and the fading rate in each case is not constant throughout the driving cycle. To see more details, the absolute SOH change rate and the associated cell current for the optimal and one-replacement strategies, for instance, are shown in Fig. 12. Due to the fact that the cells in the one-replacement strategy are more frequent to withstand relatively large discharge/charge currents, the associated SOH decrease rate is faster. This observation, in turn, demonstrates that the optimization framework for the combined HESS sizing and power management is effectively aware of the battery health. The HESS size and the power distribution between the battery and supercapacitor packs are deliberately regulated to satisfy the battery replacement requirement in the most economical manner.

5.2. Comparison with battery-only ESS option

It is quite convenient to obtain the longevity-conscious optimization result for the battery-only ESS by removing the supercapacitor model involved in Table 2. The cycle-normalized costs of the optimized HESS and battery-only ESS are compared in Fig. 13. It is obvious that the battery-only ESS is a more expensive option, inducing more hydrogen consumption and higher ESS cost. It can also be noticed that no battery replacement is still the optimal replacement strategy for the battery-only ESS. Furthermore, contrary to the HESS cost, an increasing cost of the battery-only ESS appears with regard to the number of battery replacements. The reason is that for the same cell SOH limit, i.e., Eq. (21), the size of the battery-only ESS reduces more slowly without the load-leveling assistance of supercapacitors (see Fig. 14). The power allocations between the power sources are shown in Fig. 15 for both the HESS and battery-only cases with no battery replacement. It can be observed that only the supercapacitor pack in the HESS has a stronger capability of sourcing/sinking power than does the battery-only ESS with the SOH constraint, leading to less hydrogen

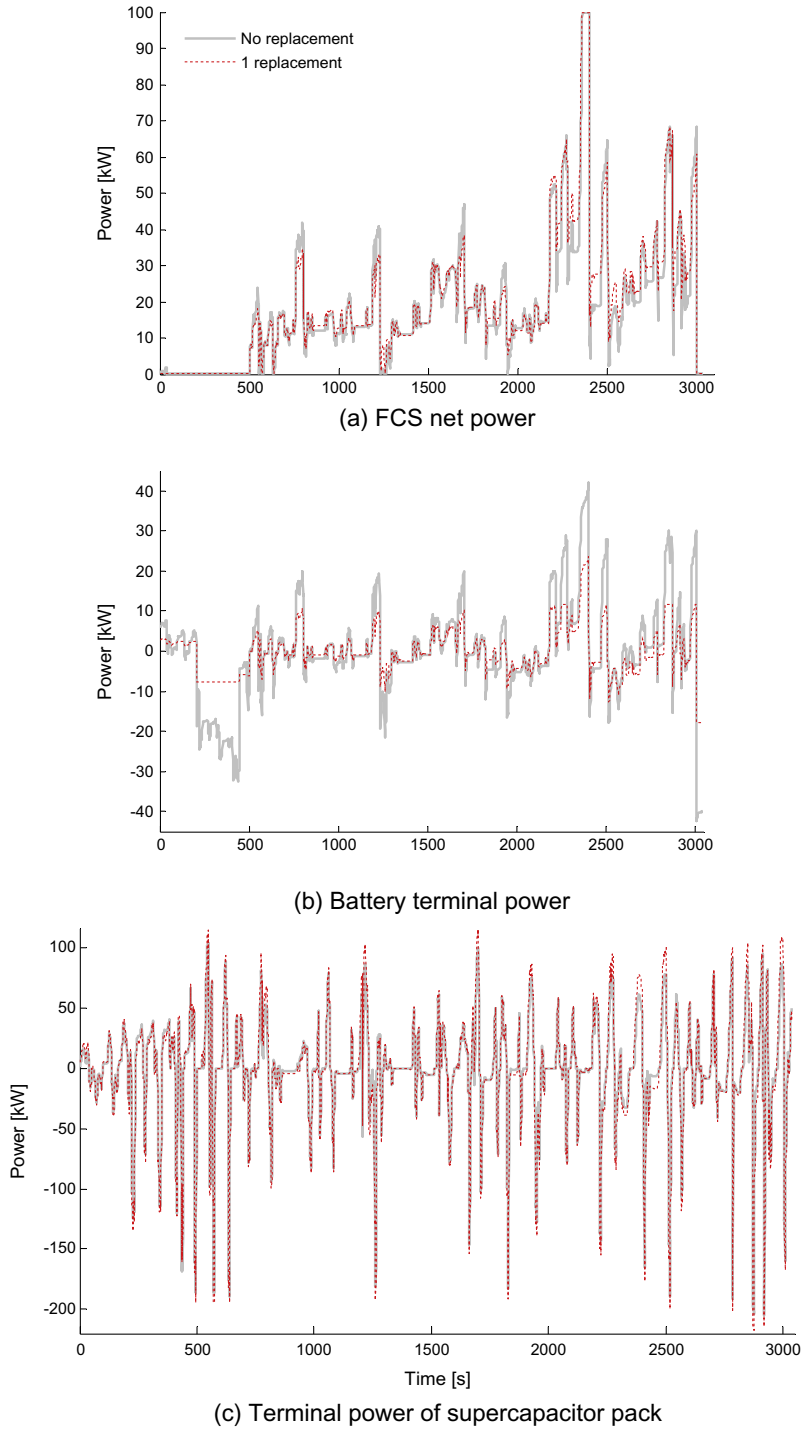

Fig. 10. Optimal power allocation between FCS and HESS: (a) FCS net power; (b) battery terminal power; and (c) terminal power of supercapacitor pack. The strategy with no battery replacement is compared to the one-replacement case.

consumption. The SOH trajectories, the SOH change rates, and the cell currents are illustrated in Fig. 16 for both cases as well. The battery-only ESS shows the same average rate of SOH decline as the HESS at the expense of a considerably larger battery pack (approximately 3.3 times of the one in the HESS). The absence of supercapacitors causes more transient cell current for the battery-only ESS, and the associated SOH change rate is more frequently altered.

The computational costs of the optimization for both the HESS and battery-only ESS cases are given in Table 5 where an averaged time for ten optimizations with different battery replacement numbers is accounted for. It is evident that the convex optimization method is extremely computationally efficient. Only about two minutes were needed to optimize both the HESS size and the power management of the hybrid bus (a very complicated system with three states). Additionally, by examining the computational time for the battery-only ESS case with two system states, it can be corroborated that the convex programming approach is not subject to "curse of dimensionality".

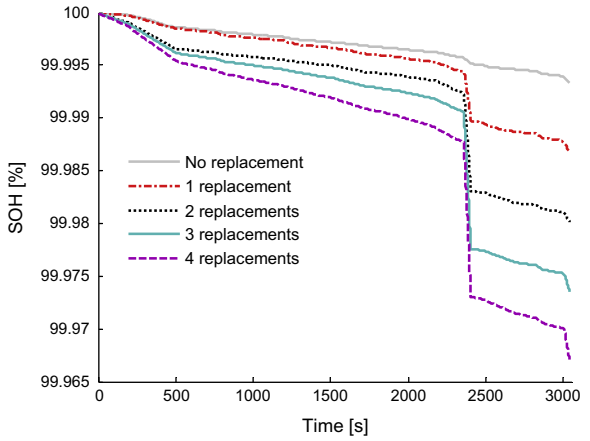

Fig. 11. Battery SOH trajectories under different replacement strategies.

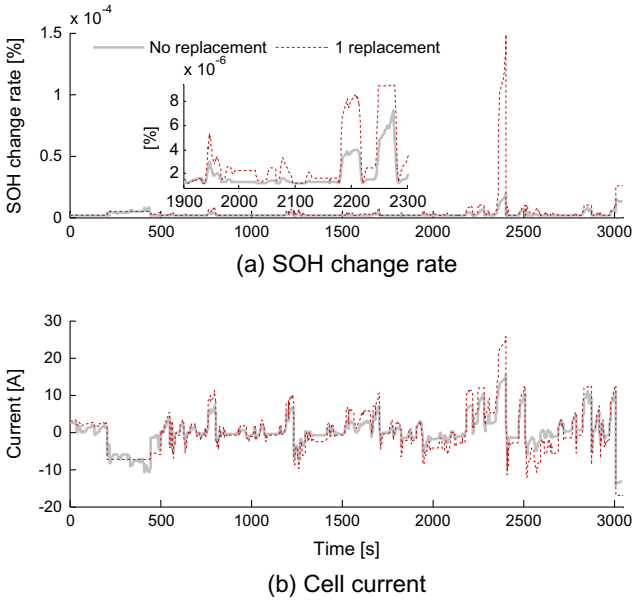

Fig. 12. SOH change rate and cell current: (a) SOH change rate; and (b) cell current.

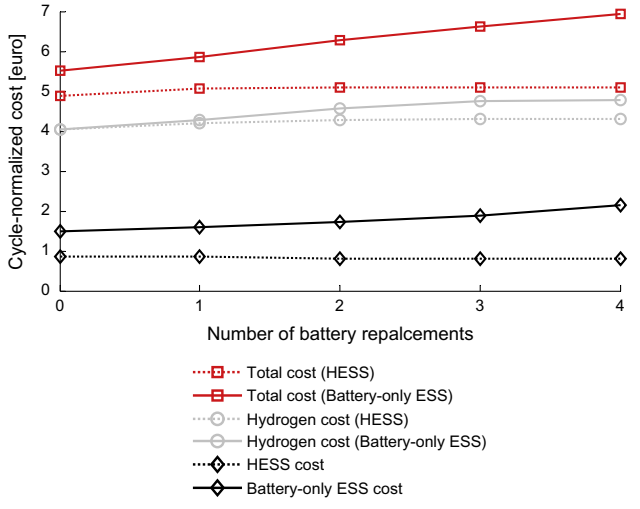

Fig. 13. Comparison between the HESS and battery-only ESS in terms of cycle-normalized costs.

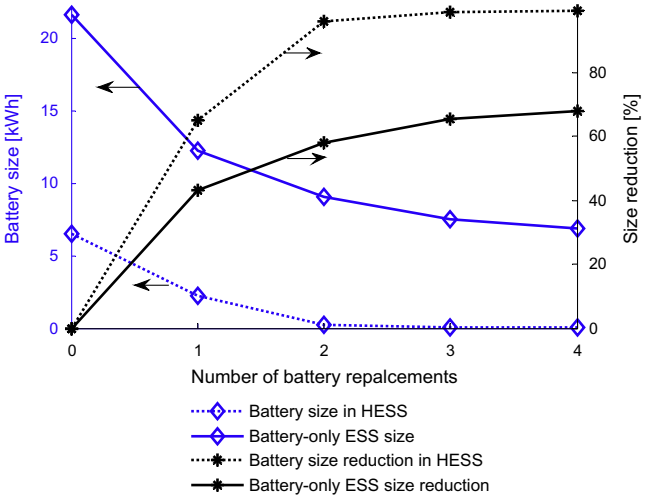

Fig. 14. Comparison between the HESS and battery-only ESS in terms of the battery size.

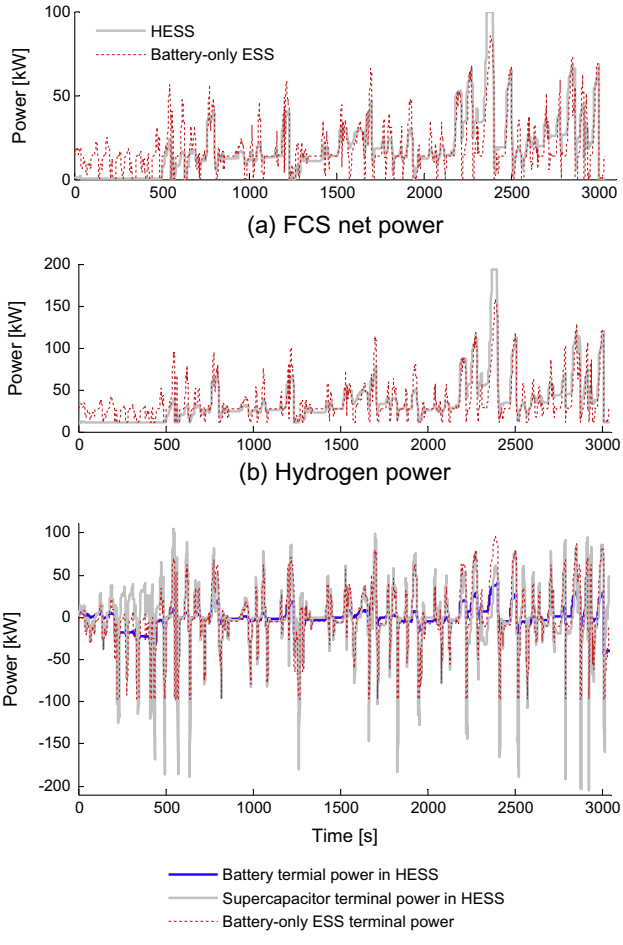

Fig. 15. Power splits between the power sources for both the HESS and battery-only options with no battery replacement: (a) FCS net power; (b) hydrogen power; and (c) ESS terminal power.

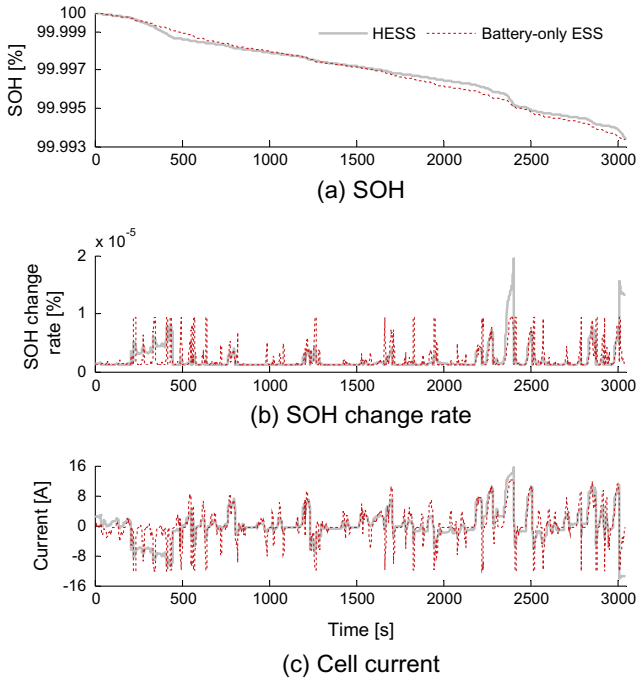

Fig. 16. SOH trajectories, change rates, and cell currents for both the HESS and battery-only options with no battery replacement: (a) SOH trajectory; (b) SOH change rate; and (c) cell current.

Table 5
Computational time of the convex optimization.

ESS	HESS	Battery-only ESS
[a]Time (s)	111.7	68.9

[a] A 2.3 GHz microprocessor with 4 GB RAM was used.

6. Comparison with optimization scenario neglecting battery SOH

With the rapid development of chemistry, more mature manufacturing techniques, and more sophisticated circuitry and management systems, it is reasonable to believe that the durability of lithium-ion batteries will be continually improved. As argued in [38], it is highly possible that the lifetime of advanced lithium-ion batteries will be adequate for automotive applications in the future. In the envisioned ideal scenario, lithium-ion batteries are allowed to be operated in a similar way to supercapacitors, i.e., an intentional power regulation for health protection is unnecessary. Also, the ideal scenario was often considered in the relevant literature to provide preliminary insights into component sizing and power management of electrified powertrains. If the battery-health-perceptive scenario described in the forgoing sections represents a solution to the current level of battery technology, an interesting question arises: how does the current solution differ from the ideal one? This section is aimed at answering this question.

The optimization outcome in the ideal scenario can be easily acquired by getting rid of the battery SOH model in the Table 2. The comparison results between the longevity-conscious scenario (with the optimal replacement strategy) and the ideal one are illustrated in Fig. 17 for both the HESS and battery-only ESS options. It is clear that the total cost is smaller in the ideal scenario, which is attributed to slightly reduced hydrogen consumption and more obvious ESS cost decrease. This observation, in turn, reflects that the battery technology advancement, particularly the durability enhancement, is of great importance for improving the vehicle economy. The optimized HESS and battery-only ESS sizes in both scenarios are compared in Fig. 18. For the battery-only ESS, the battery size in the ideal scenario is significantly smaller, owing to larger admissible discharge/charge power without the SOH constraint. For the HESS, the supercapacitor size is reduced in the ideal scenario, whereas the battery size is enlarged. It seems more economical to use more battery cells but less supercapacitor cells in the HESS in the ideal scenario. The reason is twofold: (1) the supercapacitor price per cell (20 Euros) is about three times of the battery cell price (6.8 Euros), notwithstanding an extremely high power density, and (2) the A123 lithium–iron–phosphate battery is able to deliver/absorb high power without the SOH constraint.

The battery cell currents of the HESS and battery-only ESS options for both scenarios are shown in Fig. 19. Obviously, the cell currents for both the HESS and the battery-only ESS when taking the SOH constraint into account are much smaller and smoother. Therefore, a larger and more expensive ESS (see Fig. 17) is needed to optimize the bus power management (hydrogen economy) in the longevity-conscious scenario.

7. Further discussion

Identifying battery degradation mechanisms is tremendously difficult and challenging even in the electrochemistry community, as a result of numerous intricate influencing factors. Formulation and parameterization of a complete battery aging model in a generic form is hence still an open issue until now, even though enormous efforts have been made to characterize the dynamics of battery aging in the battery area. For the purpose of a system-level simulation and optimization, a semi-empirical battery wear model from [29] with a moderate complexity is here utilized, in which the interdependence of capacity fade on current rate, energy throughput, and temperature is captured. Several effects are certainly neglected in the model, such as distinguishing the impacts of charge and discharge on the battery capacity loss and a portrayal of power fade. The model, however, can be conveniently integrated into the convex optimization framework, and the optimization results are useful and valuable to the battery-health-conscious HESS integration, dimensioning, and control from a system-level perspective, in particular at an initial or intermediate exploratory stage of the hybrid bus powertrain. When a better battery wear model is available, attempts to incorporating it into the convex optimization framework could be a focus of our future investigations.

Although a specific fuel cell/HESS hybrid electric bus driven on a bus line in Gothenburg, Sweden, is discussed, the convex optimization methodology applies to sizing and power management problems for HEVs/PHEVs with different topologies driven on discrepant routes [25]. The optimization result, nevertheless, may vary, e.g., the optimal battery replacement strategy.

The paper is concentrated on on-board HESS integration, sizing, and control for fuel cell hybrid propulsion systems. Consequently, FCS sizing is not considered. This is, however, acceptable and reasonable, since sometimes the powertrain integrators only have certain FCSs with fixed sizes. Moreover, the convex optimization framework is readily extendible to FCS sizing problem. The basic idea is to add a sizing factor for linear FCS scaling while preserving convexity. It has been proven in [39] that the FCS size can be effectively optimized. A Matlab-based toolbox for several instructive examples on convex optimization of hybrid powertrains (including FCS sizing problem) is accessible at the following website:

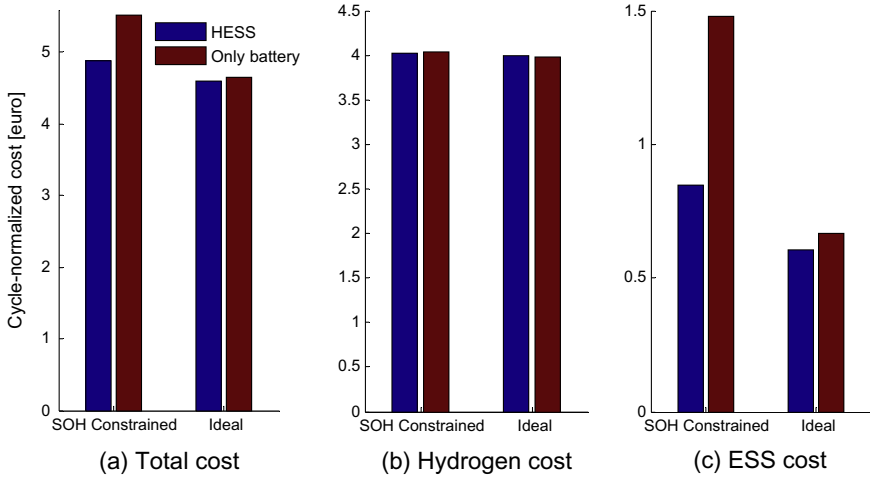

Fig. 17. Comparison results between the longevity-conscious scenario (with the optimal replacement strategy) and the ideal one for both the HESS and battery-only ESS options: (a) total cost; (b) hydrogen cost; and (c) ESS cost.

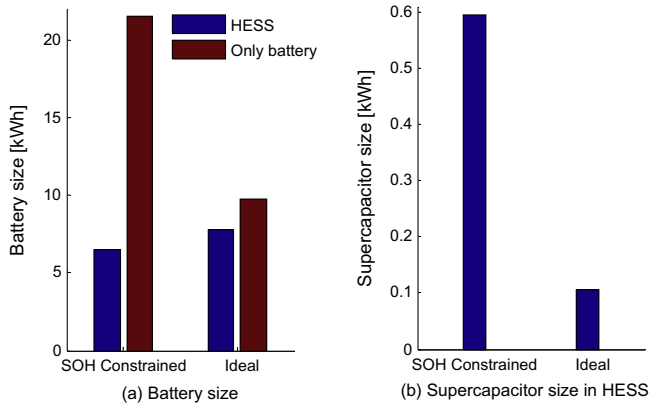

Fig. 18. Optimized HESS and battery-only ESS sizes for the longevity-conscious scenario (with the optimal replacement strategy) and the ideal one: (a) battery size; and (b) supercapacitor size.

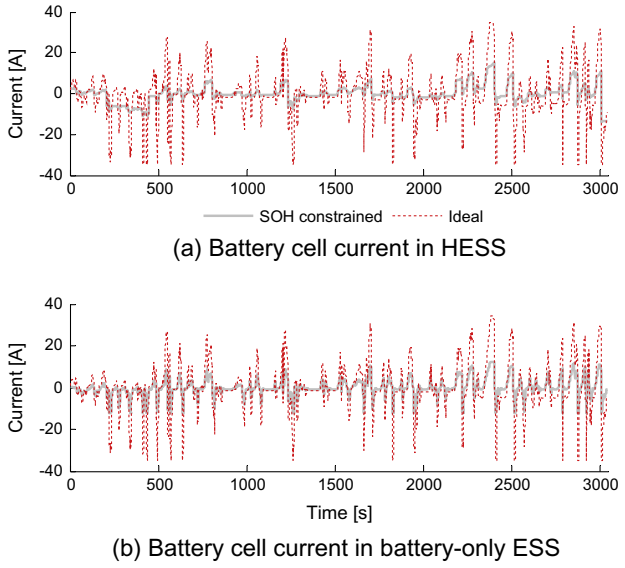

Fig. 19. Battery cell currents for the longevity-conscious scenario (with the optimal replacement strategy) and the ideal one: (a) HESS; and (b) battery-only ESS.

<http://publications.lib.chalmers.se/publication/192858-cones-matlab-code-for-convex-optimization-in-electromobility-studies>.

8. Conclusions

This paper discusses the optimal HESS dimensioning and energy management of a fuel cell hybrid electric bus operated in Gothenburg, Sweden. A simple but useful battery SOH model is incorporated into the highly efficient convex programming framework to attain the optimal HESS dimension and power management in the context of battery aging. In the optimization framework, different battery replacement strategies are assessed, and the HESS and the battery-only ESS options are also systematically compared. The battery-longevity-conscious HESS optimization outcome is contrasted to that of an envisioned ideal scenario assuming that the battery lifespan is sufficient over the bus service period without additional health-related power regulation.

The important findings for real-world powertrain design and control are summarized below:

(1) As the battery replacement number increases, the economy of the fuel cell/HESS hybrid electric bus becomes poorer. The most cost-effective (optimal) replacement strategy is thus to use a relatively large battery in the HESS guaranteeing no battery replacement over the bus service period.
(2) The comparison with the battery-only ESS in the battery-longevity-aware optimization scenario indicates that the HESS is a more economical option with less hydrogen consumption and lower ESS cost, given the same battery replacement strategy.
(3) The economy deviation of the bus between the battery-longevity-aware and envisioned ideal optimization scenarios is quantified, which highlights the importance of the battery durability improvement for increasing the vehicle economy.
(4) The convex optimization methodology is very computationally efficient. Only around two minutes have been taken to achieve the optimal HESS size and power management of the hybrid bus considering the battery SOH constraint (a highly complicated system with three states). It is also certified that the convex programming approach is not subject to "curse of dimensionality" when optimizing the electrified bus powertrain.

Acknowledgement

This work was in part supported by the Swedish Energy Agency, and the Swedish Hybrid Vehicle Center, and the Chalmers Energy Initiative.

References

[1] Chung W, Zhou G, Yeung IMH. A study of energy efficiency of transport sector in China from 2003 to 2009. Appl Energy 2013;112:1066–77.
[2] Juul N, Meibom P. Road transport and power system scenarios for Northern Europe in 2030. Appl Energy 2012;92:573–82.
[3] Hou C, Ouyang M, Xu L, Wang H. Approximate Pontryagin's minimum principle applied to the energy management of plug-in hybrid electric vehicles. Appl Energy 2014;115:174–89.
[4] Chen BC, Wu YY, Tsai HC. Design and analysis of power management strategy for range extended electric vehicle using dynamic programming. Appl Energy 2014;113:1764–74.
[5] Burke A. Batteries and ultracapacitors for electric, hybrid, and fuel cell vehicles. Proc IEEE 2007;95:806–20.
[6] Mi C, Masrur MA, Gao DW. Hybrid electric vehicles: principles and applications with practical perspectives. West Sussex: John Wiley & Sons; 2011.
[7] Ehsani M, Gao Y, Gay SE, Emadi A. Modern electric, hybrid electric, and fuel cell vehicles: fundamentals, theory, and design. 2nd ed. Boca Raton: CRC Press; 2009.
[8] Lukic SM, Cao J, Bansal RC, Rodriguez F, Emadi A. Energy storage systems for automotive applications. IEEE Trans Ind Electron 2008;55:2258–67.
[9] Khaligh A, Li Z. Battery, ultracapacitor, fuel cell, and hybrid energy storage systems for electric, hybrid electric, fuel cell, and plug-in hybrid electric vehicles: state of the art. IEEE Trans Veh Technol 2010;59:2806–14.
[10] Burke A, Miller M, Zhao H. Lithium batteries and ultracapacitors alone and in combination in hybrid vehicles: fuel economy and battery stress reduction advantages. In: Proceedings of the 25th world battery, hybrid and fuel cell electric vehicle symposium & exhibition (EVS25), 5–9 November, Shenzhen, China; 2010.
[11] Pan C, Chen L, Chen L, Huang C, Xie M. Research on energy management of dual energy storage system based on the simulation of urban driving schedules. Int J Electr Power 2013;44:37–42.
[12] He H, Xiong R, Zhao K, Liu Z. Energy management strategy research on a hybrid power system by hardware-in-loop experiments. Appl Energy 2013;112:1311–7.
[13] Sciarretta A, Back M, Guzzella L. Optimal control of parallel hybrid electric vehicles. IEEE Trans Control Syst Technol 2004;12:352–63.
[14] Guzzella L, Sciarretta A. Vehicle propulsion systems: introduction to modeling and optimization. 3rd ed. Berlin: Springer; 2013.
[15] Serrao L, Onori S, Rizzoni G. A comparative analysis of energy management strategies for hybrid electric vehicles. ASME J Dyn Syst Meas Control 2011;133:031012-1–2-9.
[16] Hu X, Murgovski N, Johannesson L, Egardt B. Energy efficiency analysis of a series plug-in hybrid electric bus with different energy management strategies and battery sizes. Appl Energy 2013;111:1001–9.
[17] Elbert P, Ebbesen S, Guzzella L. Economic viability of battery load-leveling in hybrid electric vehicles using supercapacitors. In: Proceedings of international scientific conference on hybrid and electric vehicles (RHEVE 2011), 6–7 December, Rueil-Malmaison, France; 2011.
[18] Kim MJ, Peng H. Power management and design optimization of fuel cell/battery hybrid vehicles. J Power Sour 2007;165:819–32.
[19] Ebbesen S, Dönitz C, Guzzella L. Particle swarm optimization for hybrid electric drive-train sizing. Int J Veh Des 2012;58:181–99.
[20] Murgovski N. Optimal powertrain dimensioning and potential assessment of hybrid electric vehicles. Ph.D. Dissertation. Chalmers University of Technology, Gothenburg, Sweden; 2012.
[21] Hung YH, Wu CH. An integrated optimization approach for a hybrid energy system in electric vehicles. Appl Energy 2012;98:479–90.
[22] de Castro R, Pinto C, Araújo RE, Melo P, Freitas D. Optimal sizing and energy management of hybrid storage systems. In: Proceedings of IEEE vehicle power and propulsion conference (VPPC 2012), 9–12 October, Seoul, South Korea; 2012. p. 321–6.
[23] Hu X, Murgovski N, Johannesson LM, Egardt B. Comparison of three electrochemical energy buffers applied to a hybrid bus powertrain with simultaneous optimal sizing and energy management. IEEE Trans Intell Trans Syst 2014. http://dx.doi.org/10.1109/TITS.2013.2294675.
[24] Murgovski N, Johannesson LM, Sjöberg J. Engine on/off control for dimensioning hybrid electric powertrains via convex optimization. IEEE Trans Veh Technol 2013;62:2949–62.
[25] Egardt B, Murgovski N, Pourabdollah M, Johannesson LM. Electromobility studies based on convex optimization: design and control issues regarding vehicle electrification. IEEE Control Syst Mag 2014;34:32–49.
[26] Tazelaar E, Veenhuizen B, van den Bosch P, Grimminck M. Analytical solution of the energy management for fuel cell hybrid propulsion systems. IEEE Trans Veh Technol 2012;61:1986–98.
[27] Odeim F, Roes J, Wülbeck L, Heinzel A. Power management optimization of fuel cell/battery hybrid vehicles with experimental validation. J Power Sour 2014;252:333–43.
[28] Gaines L, Cuenca R. Costs of lithium-ion batteries for vehicles. Technical Report, Center for Transportation Research at Argonne National Laboratory, U.S. Department of Energy; 2000.
[29] Wang J, Liu P, Hicks-Garner J, Sherman E, Soukiazian S, Verbrugge M, et al. Cycle-life model for graphite–$LiFePO_4$ cells. J Power Sour 2011;196:3942–8.
[30] Ebbesen S, Elbert P, Guzzella L. Battery state-of-health perceptive energy management for hybrid electric vehicles. IEEE Trans Veh Technol 2012;61:2893–900.
[31] Johannesson L, Murgovski N, Ebbesen S, Egardt B, Gelso E, Hellgren J. Including a battery State of Health model in the HEV component sizing and optimal control problem. In: Proceedings of the 7th IFAC symposium on advances in automotive control (AAC 2013), 4–7 September, Tokyo, Japan; 2013. p. 398–403.
[32] Boyd S, Vandenberghe L. Convex optimization. Cambridge: Cambridge University Press; 2004.
[33] Grant M, Boyd S. CVX: Matlab software for disciplined convex programming, version 1.21. <http://cvxr.com/cvx> [accessed by May 2010].
[34] Labit Y, Peaucelle D, Henrion D. SeDuMi interface 1.02: a tool for solving LMI problems with SeDuMi. In: Proceedings of IEEE international symposium on computer aided control system design, 18–20 September, Glasgow, Scotland, U.K.; 2002. p. 272–7.
[35] Hulteberg C, Aagesen D. Hydrogen production for refuelling applications. Technical Report (Report No. SGC-R-210-SE), Swedish Gas Centre (SGC); 2009.
[36] <http://www.robotcombat.com/products/images/bp_configs/pdf/ANR26650M1.pdf> [accessed by June 2011].
[37] <http://www.maxwell.com/products/ultracapacitors/docs/datasheet_k2_series_1015370.pdf> [accessed by July 2010].
[38] Pollet BG, Staffell I, Shang J. Current status of hybrid, battery and fuel cell electric vehicles: from electrochemistry to market prospects. Electrochim Acta 2012;84:235–49.
[39] Murgovski N, Hu X, Johannesson L, Egardt B. Combined design and control optimization of hybrid vehicles. In: Conejo A, Yan J, editors. Electric car and hybrid car. Handbook of clean energy systems, vol. 4. West Sussex: Wiley; 2014 [in press].